Phase-locked multicore all-fiber lasers: modeling and experimental investigation

L. Li,[1,*] A. Schülzgen,[1] H. Li,[2] V. L. Temyanko,[1] J. V. Moloney,[2] and N. Peyghambarian[1]

[1]*College of Optical Sciences, University of Arizona, Tucson, Arizona 85721, USA*
[2]*Arizona Center for Mathematical Sciences, University of Arizona, Tucson, Arizona 85721, USA*
[*]*Corresponding author: lli@email.arizona.edu*

Received November 1, 2006; revised March 11, 2007; accepted March 12, 2007;
posted April 10, 2007 (Doc. ID 76656); published July 19, 2007

A systematic study on a compact, novel phase-locked multicore fiber laser device that is based on a truly all-fiber approach is presented. Supermode selection inside this monolithic fiber device is numerically analyzed, and multicore fiber lasers operating explicitly at the in-phase supermode are experimentally demonstrated.

OCIS codes: 140.3510, 140.3290, 070.6760.

1. INTRODUCTION

Coherent beam combining of fiber lasers, a critical technique toward developing compact high-power lasers with high brightness, has inspired the recent emergence of fibers with multiple active cores [1,2]. A multicore fiber (MCF) generally has a larger emitting area compared with a monocore fiber; meanwhile, as multiple emitters are distributed in an array and separated by passive regions, the thermal and stress problems encountered at high-power levels are alleviated [3]. However, if each emitter in the core array oscillates independently with random phase relationship, the output beam will diverge as fast as an individual emitter does [2]. The low-brightness output beams from the incoherently combined core arrays will not be very beneficial for practical applications.

To coherently combine the individual emitters and obtain a high-brightness output beam from the array, the relative phase between adjacent emitters requires to be locked, as demonstrated in early semiconductor laser arrays [4–13]. For a typical MCF, the core array is either distributed in a ring, or a densely packed two-dimensional isometric pattern. In both scenarios, each single-mode core evanescently couples with its neighboring cores, and different supermodes are formed and characterized by the fixed (locked) phase difference between adjacent emitters. Each supermode has its own distinctive intensity distribution and diffraction property, but only the fundamental in-phase supermode, i.e., all cores locked in the same phase, has a Gaussian-like far-field intensity distribution with an intensified central lobe of low divergence [2]. However, since mode competition exists inevitably in MCF laser cavities [14], it is equally important, as the design and manufacture of the MCF, to build a fiber laser cavity that establishes solely the in-phase mode and suppresses all higher-order modes.

To coherently combine the emissions of a core array into a phase-locked supermode, it is essential to develop a selective feedback mechanism that supports only one specific supermode with maximal gain and minimal loss while it discriminates all other modes with less gain and higher loss during cavity round trip. Among recent approaches to provide such a differential feedback, the most promising scheme is to utilize the Talbot effect [15,16], which has been demonstrated earlier with diode [17,18], microchip [19], and CO_2 waveguide [20] laser arrays. Talbot cavity MCF lasers have also been reported recently with phase-locked high-brightness output beams obtained [21–25]. However, in these MCF lasers, free-space optics, i.e., air gaps and bulk optical components, has become an inseparable part [21–25]. The presence of free-space optics in a fiber laser cavity is practically undesirable, because it not only substantially expands the device size from a single piece of fiber to a bulky open-space setup but also introduces more cavity loss. Furthermore, serious stability issues can occur at high-power laser operation, e.g., thermal or environmental disturbances can easily affect the crucial and delicate cavity alignment. Therefore, it is a strong preference to eliminate any free-space optics and force the supermode selection to occur inside a confined waveguide, ideally, within an optical fiber. This will result in a truly all-fiber phase-locked MCF laser, which is free of optical alignment and robust against external disturbances.

In earlier all-fiber approaches to phase lock the emissions of a core array, the out-of-phase supermode has been selected by either an annular waveguide [26] or a fiber mirror [27,28], while the in-phase supermode amplification has been achieved with a pulsed Gaussian beam [29]. Recently, we have reported, to the best of our knowledge, a novel compact all-fiber MCF laser that solely oscillates at the in-phase mode, with the complete device being a single fiber chain of ~10 cm in length [30]. In this monolithic fiber device, the in-phase mode is selected by multimode noncore optical fibers spliced to the active MCF, resulting in complete elimination of free-space and bulk

optics. This all-fiber modal selection approach not only drastically simplifies the cavity geometry but also results in stable and robust phase-locked laser operation.

In this paper, we present a detailed and systematic study on the all-fiber phase-locked MCF lasers. In Section 2, we numerically analyze the propagation, diffraction, and coupling characteristics of the supermodes of a 19-core MCF (MC19) inside a multimode noncore fiber (NCF) and compare with the free-space optics case utilizing air spacing and a bulk mirror. Our simulation indicates an optimal NCF length range to select the in-phase mode, which is confirmed in the experimental investigation in Section 3. The MC19 lasers are fabricated and tested with spliced NCF of various lengths. The modal selectivity is further improved by adding NCF at both ends of the MC19 and high-quality output beams with Gaussian-like intensity distributions are observed in the far field. In Section 4, we present results of MCF lasers with an upgraded 37-core array and experimentally demonstrate the in-phase mode oscillation utilizing the same all-fiber approach. Finally, we draw conclusions from this study in Section 5.

2. NUMERICAL ANALYSIS OF THE IN-FIBER SUPERMODE SELECTION

One common and effective approach to provide a differential feedback for MCF supermode selection is to use the free-space Talbot effect, which states that a coherent one-dimensional periodic wave reproduces its initial field distribution after it propagates a certain distance. This characteristic distance is called the Talbot distance,

$$Z_T = 2\Lambda^2/\lambda, \tag{1}$$

where λ is the free-space wavelength and Λ is the periodicity of the initial field.

To utilize the Talbot effect for supermode selection in a MCF laser cavity, a typical setup is to place a mirror at a distance Z_M from the MCF, as illustrated in Fig. 1(a). The MCF supermodes exit the facet at $Z=0$ and re-enter the MCF after completing a round trip between the mirror and the facet. When the mirror position Z_M matches $Z_T/2$ of a MCF supermode i, this mode is to have the maximal amplitude reflection coefficient $\gamma_i(Z=2Z_M)$ [22]:

$$\gamma_i(Z) = \frac{\left| \int_{-\infty}^{\infty} A_i^*(x,y,0) A_i(x,y,Z) \mathrm{d}x\mathrm{d}y \right|}{\left| \int_{-\infty}^{\infty} A_i(x,y,0) A_i^*(x,y,0) \mathrm{d}x\mathrm{d}y \right|}, \tag{2}$$

where $A_i(x,y,0)$ represents the initial field, $A_i(x,y,Z)$ denotes the reflected field, and the ratio of the overlapping integrals $\gamma_i(Z)$ defines the modal amplitude reflection (coupling) coefficient. Therefore, by placing the mirror at $Z_T/2$ of the in-phase mode (or at multiples of $Z_T/2$), the fundamental mode will have the maximum $\gamma_i(Z)$ and all higher-order modes suffer larger diffraction and coupling losses. Supermode selection has been successfully demonstrated by this approach with ring-distributed step-index and photonic crystal MCFs [22,23].

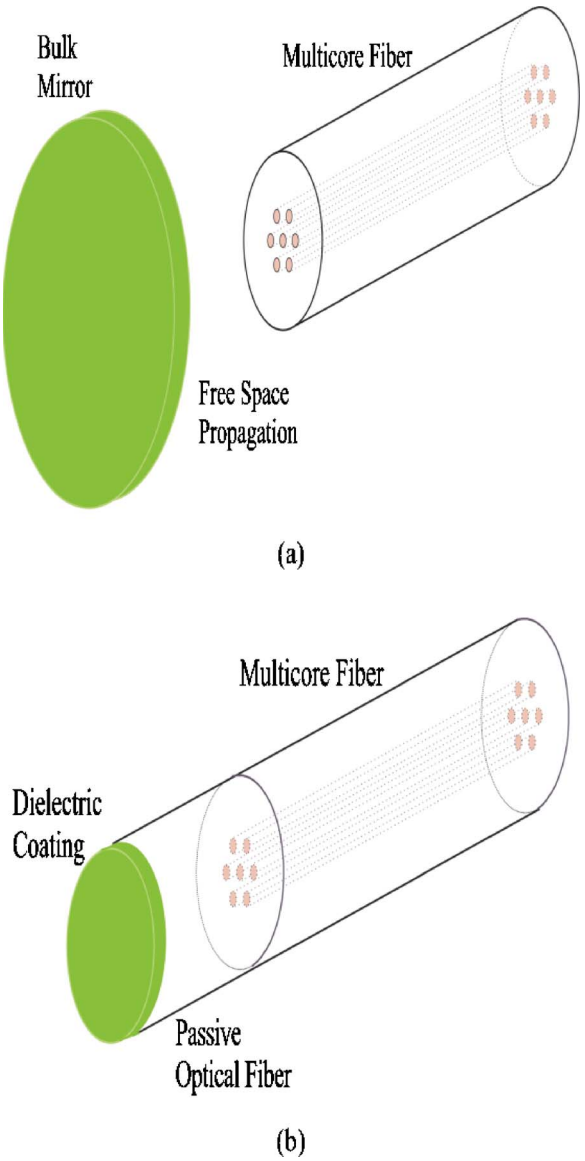

Fig. 1. (Color online) Supermode selection in MCF laser cavity. (a) A free-space Talbot cavity, (b) an all-fiber cavity utilizing a mirror-coated passive optical fiber.

To replace the inconvenient air gap and bulk mirror in the previous Talbot cavity fiber laser, a multimode passive optical fiber that could be spliced to the active MCF appears to be an attractive choice for the construction of the desirable all-fiber phase-locked laser, as shown in Fig. 1(b). Inside the extended passive fiber section, the confined supermodes exit and couple back into the MCF after completing the round trip. If the radial dimension of the passive fiber is sufficiently large and the supermodes never expand enough to reach the lateral boundary during the round trip, this approach is essentially identical to the free-space Talbot cavity method, except for replacing λ in Eq. (1) with λ/n, with n being the refractive index of the fiber material. However, to facilitate the practical fiber fusion splice process, the passive fiber is typically chosen to have the same or comparable dimension as the MCF, which is not large enough to be treated as the free-space medium and its particular modal properties must be considered. Therefore, inside the multimode passive fi-

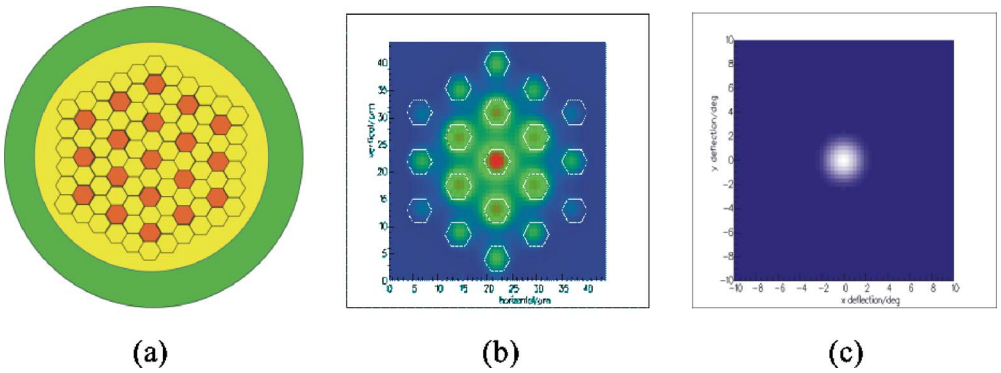

Fig. 2. (Color online) Isometrically distributed 19-core MCF. (a) The cross section; (b) simulated near-field and (c) far-field intensity distributions of the in-phase supermode.

ber, supermode selection becomes a combined result of diffraction, Talbot effect, and multimode interference (MMI) that has been stated responsible for the field reconstruction of injected MCF modes [31]. Our numerical analysis in this section will find pronounced differences in the amplitude reflection coefficients between propagation in the bulk medium and inside a multimode fiber.

We start with a MC19 that has a two-dimensional isometric core array, as shown in Fig. 2(a). Each single-mode core has a diameter of 7.6 μm and a numerical aperture of 0.12 at 1.5 μm. The double-cladded MC19 has an outer diameter (OD) of 200 μm and the inner cladding is primarily for pump light confining. Supermodes of this MC19 have been calculated utilizing a finite-element method (FEM) [32], and the near- and far-field intensity distributions of the fundamental in-phase mode are shown in Figs. 2(b) and 2(c), respectively. The far-field Gaussian-like beam has a full angular spread of 0.04 rad.

To select the in-phase mode with an all-fiber device, we choose a passive NCF having the same OD of 200 μm. We assume one end of the NCF is spliced to the MC19, and the other end is perpendicularly cleaved and coated with a mirror of 100% reflectivity, as shown in Fig. 1(b). We assume no splicing and scattering loss to simplify the calculation.

A mode expansion method (MPM) is used to calculate $\gamma_i(Z)$ of every supermode propagating inside the NCF. We first launch and project a MC19 supermode onto an eigenmode basis of the NCF. Then we calculate the propagating property of every excited eigenmode inside the NCF. Finally, at positions where we evaluate the supermode, we reconstruct the field by summing up all the excited NCF eigenmodes. Considering the large diameter of the NCF as well as the substantial refractive index difference between the NCF and the surrounding air, the NCF is highly multimode. One would thus expect tens of thousands of NCF eigenmodes are needed in the basis to validate the MPM, which makes the calculation infeasible. However, we have in fact found that >99.9% of the energy of a launched MC19 supermode is contained in only several hundred excited NCF eigenmodes, which greatly reduces the calculation volume. Our numerical method is still under improvement, and further details of the MPM will be discussed in future publications.

To understand the supermode selection inside the NCF, we first compare the difference in $\gamma_i(Z)$ between inside the NCF [Fig. 1(b)] and in the free-space Talbot cavity [Fig. 1(a)]. Choosing the in-phase mode as an example, we obtain $\gamma_1(Z)$ in the NCF by MPM, shown as the dashed curve in Fig. 3. For the free-space Talbot cavity, we also assume a 100% reflecting mirror, assign the free space with the same refractive index as the NCF, and utilize a vectorial diffraction method to calculate $\gamma_1(Z)$. The result is shown as the solid curve in Fig. 3. The two curves are identical at $Z<1000$ μm where the in-phase mode has not expanded large enough to reach the NCF lateral boundary. This coincidence confirms the validity of the MPM by the fully vectorial diffraction calculation. For $Z>1000$ μm, the free-space curve monotonously declines, while the NCF curve shows a strong oscillatory behavior resulting from the MMI self-imaging effect [33]. The high maxima in the NCF $\gamma_1(Z)$ curve from $Z=\sim 2200$ to 3200 μm indicate a potentially more efficient all-fiber laser device compared with the free-space Talbot cavity laser.

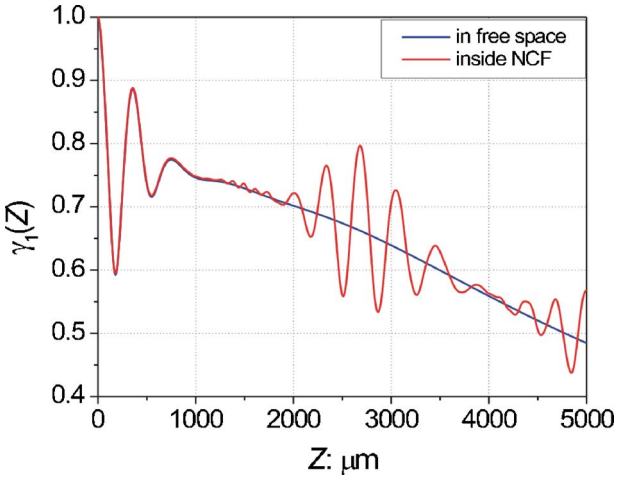

Fig. 3. (Color online) Calculated $\gamma_1(Z)$ of the MC19 in-phase supermode: in free space (solid curve) and inside NCF (dashed curve).

The $\gamma_i(Z)$ of all MC19 supermodes inside the NCF has been calculated. Several selected $\gamma_i(Z)$ of higher-order modes, along with $\gamma_1(Z)$, are shown in Fig. 4(a). It is clearly observed that once Z reaches ~4000 μm, at least one higher-order $\gamma_i(Z)$ catches up with or even surmounts $\gamma_1(Z)$. This behavior indeed deviates from the free-space

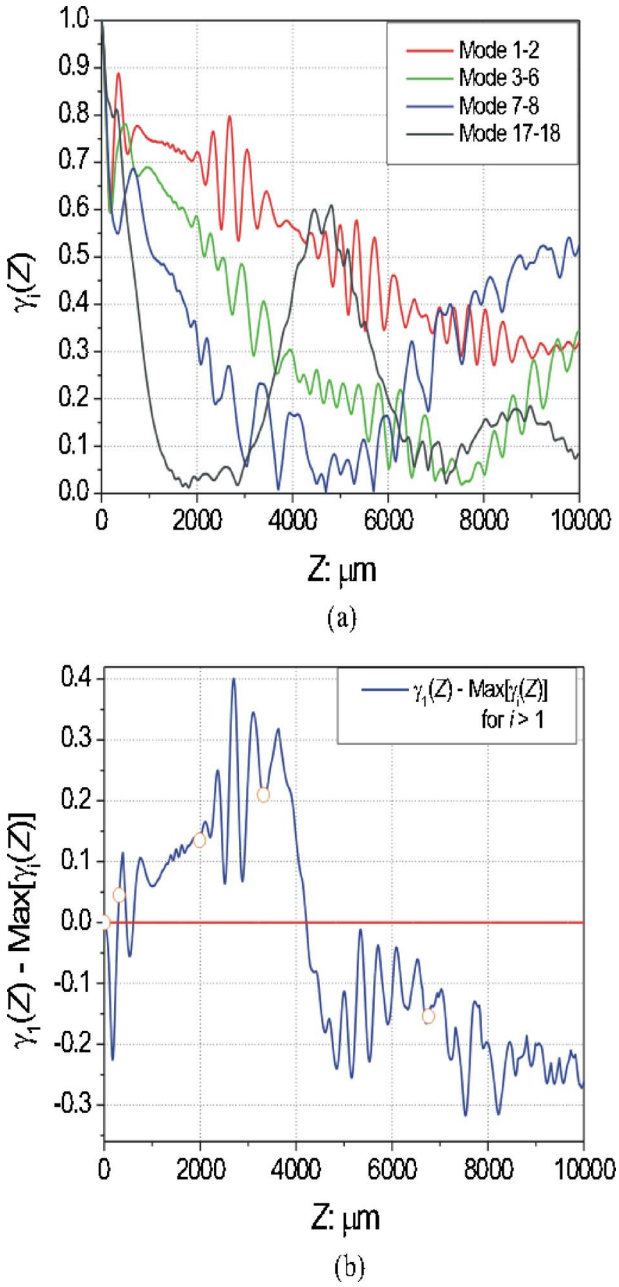

Fig. 4. (Color online) (a) Calculated $\gamma_i(Z)$ of selected MC19 supermodes inside the NCF. (b) Difference between $\gamma_1(Z)$ and the maximum of $\gamma_i(Z)$ of all higher-order modes: open circles denote positions for later experimental investigation.

Talbot cavity case, in which once the mirror is pulled sufficiently away from the MCF facet, the larger the separation, the better the selection of the in-phase mode.

Finally, to decide the optimal NCF length, we plot the difference between $\gamma_1(Z)$ and the maximum of all $\gamma_i(Z)$ for $i>1$, as shown in Fig. 4(b). We find that the best positive contrast between the in-phase mode and higher-order modes is achieved with Z ranging from ~1500 to 4000 μm. It is also observed that when $Z>4200$ μm, $\gamma_1(Z)$ becomes smaller than $\gamma_i(Z)$ of some higher-order modes, meaning that a longer NCF does not favor the in-phase mode selection, in striking contrast to the free-space cavity scenario.

3. EXPERIMENTAL STUDY OF THE NON-CORE-FIBER-SPLICED 19-CORE FIBER LASER

The MC19 with specifications given in Section 2 has been manufactured utilizing a similar stack-and-draw process for microstructured optical fibers [34]. The microscopic photograph of the cross section of the drawn MC19 is shown in Fig. 5(a). The MC19 is made of phosphate glasses, and the cores are heavily codoped with Er^{3+} and Yb^{3+} ions (1.5 wt. % of Er_2O_3 and 8.0 wt. % of Yb_2O_3) for compact high-power fiber laser applications [35]. An OD 200 μm NCF, also made of phosphate glass, is chosen as the modal selection element in the all-fiber laser cavity.

First, a short piece (~10 cm) of MC19 is cleaved at both ends and served as the gain medium. The high concentrations of Er^{3+} and Yb^{3+} ions in the cores ensure sufficient pump absorption even with such short fibers [35]. Then, a piece of NCF is spliced to one end of the MC19, and the other MC19 end is pumped with 975 nm laser diodes. The pump light is butt coupled into the MC19 cladding by a multimode fiber whose facet is coated with a broadband 1.5 μm high reflector. The far-field intensity pattern of the output beam is recorded on a screen set at 7.5 cm away from the cleaved NCF output end.

To determine the NCF length influence upon modal selection, we have spliced NCFs of length varying from 0 to 3500 μm (equivalent Z value doubles). The MC19 lasers with NCF lengths equivalent to $Z=0$, 312, 1984, 3320, and 6760 μm, which are marked as open circles in Fig. 4(b), have been manufactured and tested. The far-field emission patterns are shown in Figs. 5(b)–5(f). We notice, with none ($Z=0$) and short ($Z=312$ μm) NCF, where the in-phase mode is not positively distinguished, the output beam is fast spread and messy; with NCF length increased to $Z=1984$ and 3320 μm, where $\gamma_1(Z)$ is predicted with large advantage, the beam quality is observed noticeably improved; with further lengthened NCF ($Z=6760$ μm) where higher-order modes are favored, the beam quality deteriorates again. The calculated optimal NCF length range shown in Fig. 4(b) thus agrees well with experimental observations.

As shown in Figs. 5(d) and 5(e), though the on-axis intensity of the MC19 laser emission is enhanced considerably by one piece of spliced NCF, the higher-order mode contributions are still significant. To further improve the beam quality with reinforced mode selecting effect, a second piece of NCF is spliced at the MC19 pump end, in addition to the NCF at the output end [30]. The effective length of this second NCF is determined experimentally, and we have found that the optimal NCF combination for the OD 200 μm MC19 laser is with ~1700 μm long NCF at the output end and ~550 μm long NCF at the pump launching end. The far-field intensity pattern of the output beam from this MC19 laser device is shown in Fig. 6(a), as a clean on-axis spot is observed with a horizontal angular spread of ~0.04 rad, agreeing with the calculated value of the in-phase mode. Since the conventional M^2 measurement is known to be inappropriate for MCF laser array output [36], we instead use the divergence angle (angular spread) in the far field as the criterion for the beam quality. Comparing Fig. 6(a) with Fig. 5(b), the as-

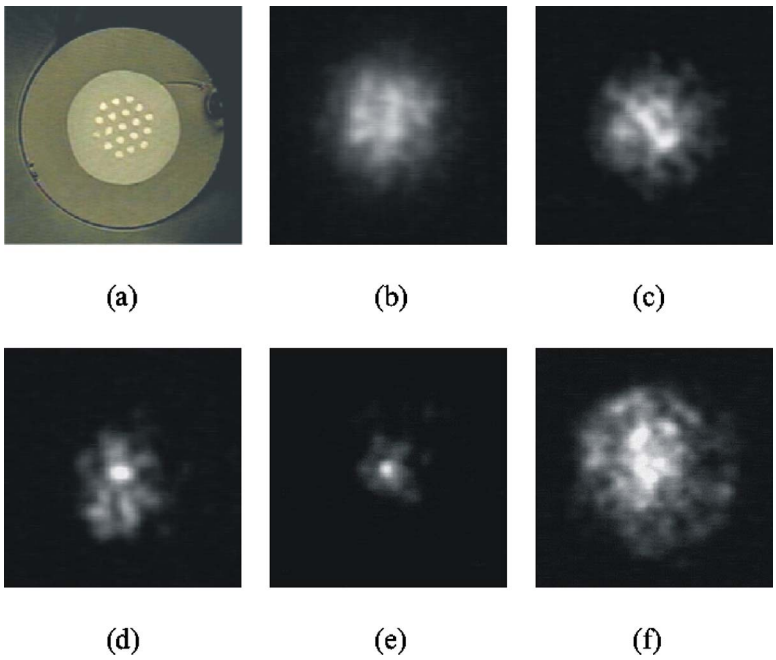

Fig. 5. (Color online) (a) Microscopic photo of the cross section of the drawn MC19. Recorded far-field emission patterns from MC19 lasers with spliced NCF of lengths equivalent to Z (μm)= (b) 0, (c) 312, (d) 1984, (e) 3320, and (f) 6760.

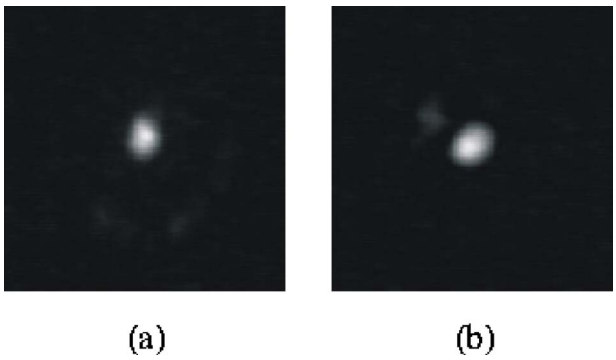

Fig. 6. Far-field emission patterns of MC19 lasers spliced with NCF at both ends. (a) MC19 of OD 200 μm; (b) MC19 of OD 125 μm.

tonishing enhancement in beam quality demonstrates the validity of our all-fiber supermode selection approach.

To note, the most effective NCF length experimentally obtained is not located exactly at the calculated oscillatory high peaks of $\gamma_1(Z)$ in Fig. 4(b). This deviation comes from the manufacturing defects of the MC19, as the irregularity of the individual cores obviously shown in Fig. 5(a). We also note the asymmetric NCF length distribution at the two MC19 ends, which is possibly due to the large pump absorption difference between the pump and output ends, inherent to the single-end pumping scheme.

The NCF mode selection approach is not limited by the fiber dimension, though we have only tested the large OD 200 μm fiber up to now. Next, another MC19 has been drawn with a smaller OD of 125 μm. It has the identical design as the larger MC19 with every dimension proportionally scaled down. A passive phosphate NCF of OD 125 μm is utilized as the mode selecting fiber. By following the same process upon the larger MC19, an all-fiber OD 125 μm MC19 laser operating at the in-phase mode is fabricated and tested, with ~210 μm long NCF spliced at the output end and ~200 μm long NCF at the pump end. The far-field intensity pattern of the output beam is shown in Fig. 6(b), and the Gaussian-like beam has a full angular spread of 0.05 rad, closely matching the theoretical value of 0.06 rad of the in-phase mode.

The demonstrated in-phase supermode oscillation of our all-fiber MCF lasers is fundamentally robust. Possible fluctuations in relative optical pass length are minimized since all cores are embedded in the same cladding. More importantly, all cores of the array are coupled optically and forced to emit collectively into one supermode. Due to this coupling, the cores cannot be treated as independent lasers with specific and varying relations among them. We do not observe any instability that might occur due to temperature gradients at high-power operation, indicating that these effects are rather small [3].

Finally, we discuss the power penalty in fiber laser performance due to extra losses introduced at the fusion splices and inside the NCF. To compare, a piece of 10 cm long OD 200 μm MC19 is used as the active medium to construct the fiber laser. To improve the overall laser efficiency, a dielectric mirror, which is highly reflective at 975 nm and has a reflectivity of ~54% at 1.5 μm, is added at the output end. A first fiber laser is tested solely with MC19 without NCF attached. A maximum output power of 16 W is obtained with a slope efficiency (SE) of 20% with respect to the launched pump power. A second MC19 laser is fabricated with both ends spliced with NCFs of lengths specified in Fig. 6(a). A maximum output power of 11 W is achieved with an SE of 14%. The signal versus pump power plots of both devices are shown in Fig. 7. The decreased efficiency of the second laser device results mainly from the relatively large splice losses between the MC19 and NCF, which could be reduced by optimizing the

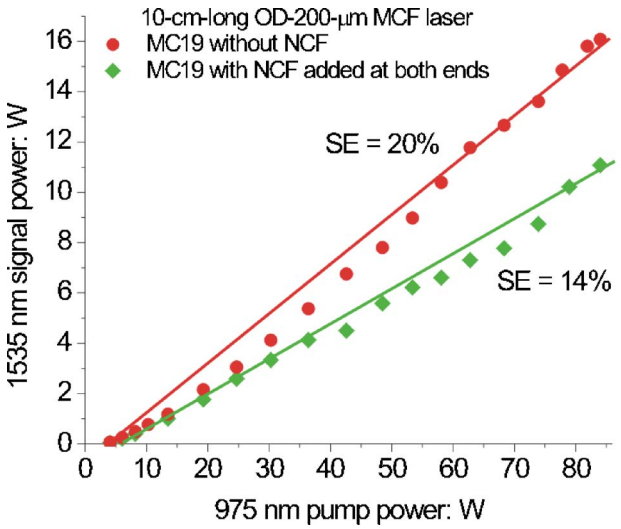

Fig. 7. (Color online) Signal versus pump power plots of 10 cm long MC19 lasers with (solid diamonds) and without (solid circles) NCF spliced.

splice process. To be noticed, with the free-space Talbot cavity phase-locked fiber lasers (utilizing the same MC19), we have not been able to achieve a SE better than 5%, which confirms the advantage of the all-fiber structure for laser efficiency.

To summarize this section, compact all-fiber phase-locked MCF lasers have been demonstrated with spliced NCFs effectively selecting the in-phase supermode. Compared with earlier phase-locked MCF lasers utilizing meter(s)-long active fibers and free-space bulk optics in the cavity, our approach provides a drastically space-saving solution and enables these active fiber sources integrable to compact photonic systems.

4. EXPANDING THE FIBER CORE ARRAY TO 37 CORES

To further explore the all-fiber supermode selection approach, in this section, we apply it to MCF with a larger-scale core array. Based on the design of the previous MC19, another ring of cores are added to form an isometrically distributed 37-core MCF (MC37), as shown in Fig. 8(a). The supermodes of the MC37 are calculated utilizing FEM [32], and for the in-phase mode, its near-field intensity distribution is shown in Fig. 8(b), and the Gaussian-shaped far-field intensity pattern is shown in Fig. 8(c).

We have drawn MC37 with two different ODs, 125 and 200 μm, respectively. The cross section of the manufactured MC37 is shown in Fig. 9(a). The far-field emission pattern from a bare MC37 laser without modal manipulation is shown in Fig. 9(b). A similar NCF-based modal selection approach, as described in Section 2, has been applied to MC37 to establish the in-phase mode oscillation. In the finalized MC37 laser devices, both ends of a piece of 10 cm long MC37 are spliced with NCFs for enhanced mode filtering effect. For the OD 125 μm MC37 laser, with NCF of $\sim$520 μm long at the output end and $\sim$925 μm long at the pump end, the recorded far-field intensity pattern is shown in Fig. 9(c). The Gaussian-like beam has a full angular spread of 0.05 rad that matches well with the calculated in-phase mode value of 0.06 rad. For the OD 200 μm MC37 laser, with 1650 μm long NCF at the output end and 3000 μm long NCF at the pump end, the far-field emission pattern is shown in Fig. 9(d). The full width at half maximum (FWHM) of the central lobe is measured to be 0.03 rad, which is identical to the theoretical value of the in-phase mode. The utilization of FWHM here is due to the remaining higher-order modes contribution in the output beam. Overall, the distinctive difference in beam quality from Fig. 9(c) and Fig. 9(d) to Fig. 9(b) is clearly observed and the effectiveness of our all-fiber modal selection technique is well demonstrated even with larger-scale core arrays.

The fabricated MC37 laser has a similar SE as that of the MC19 laser, because MC37 has smaller cores in the array resulting in almost identical active area of the two MCFs. The power scale-up of the MC37 laser could be readily achieved by expanding the individual core size in the array.

5. CONCLUSIONS

To conclude, we have presented a systematic and detailed study on a compact all-fiber approach to selectively phase lock the MCF supermodes. Both numerical analysis and experimental investigation have demonstrated that the in-phase mode could be effectively established by spliced noncore optical fibers of controlled length, with the simulation and experimentation in good agreement. This approach applies to MCFs with different outer diameters and arrays with various quantities of cores, and therefore indicates strong application potentials toward compact high-power and high-brightness laser devices.

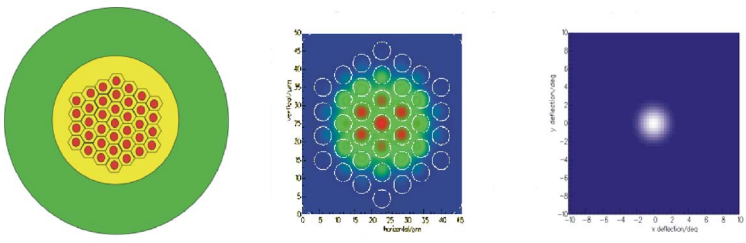

Fig. 8. (Color online) Isometrically distributed 37-core MCF. (a) The cross section; (b) simulated near-field and (c) far-field intensity distributions of the in-phase supermode.

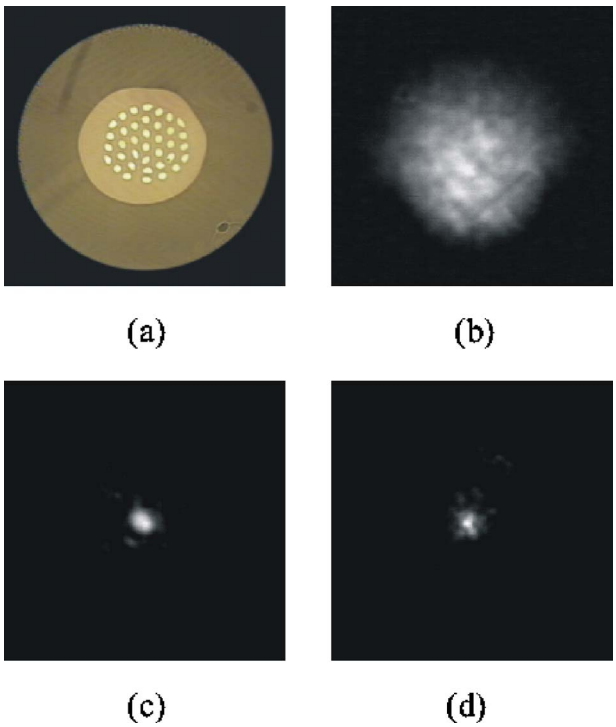

Fig. 9. (Color online) (a) Microscopic photo of the cross section of the drawn MC37. Recorded far-field emission patterns from (b) MC37 laser without NCF spliced; MC37 lasers with both ends spliced with NCF: (c) OD 125 μm fiber; and (d) OD 200 μm fiber.

ACKNOWLEDGMENTS

The authors thank S. Jiang and T. Luo of NP Photonics Inc. for providing the phosphate glasses, and E. Temyanko, S. Sabet, and Y. Merzlyak for technical support. This work is supported by the Air Force Office of Scientific Research through a Multidisciplinary Research Initiative program F49620-02-1-0380, National Sciences Foundation grant 0335101, and the state of Arizona Technology and Research Initiative Funding Photonics Initiative.

REFERENCES

1. P. Glas, M. Naumann, A. Schirrmacher, and T. Pertsch, "A cw diode-pumped single-silica fiber comprising 40 cores used as active elements for a high power fiber laser at $\lambda = 1050$ nm," in *Conference on Lasers and Electro-Optics* (Optical Society of America, 1998), pp. 113–114.
2. P. Glas, M. Naumann, A. Schirrmacher, and T. Pertsch, "The multicore fiber—a novel design for a diode pumped fiber laser," Opt. Commun. **151**, 187–195 (1998).
3. Y. Huo and P. K. Cheo, "Thermomechanical properties of high-power and high-energy Yb-doped silica fiber lasers," IEEE Photon. Technol. Lett. **16**, 759–761 (2004).
4. J. Crowe and W. Ahearn, "External cavity coupling and phase locking of gallium arsenide injection lasers," IEEE J. Quantum Electron. **4**, 169–172 (1968).
5. J. E. Ripper and T. L. Paoli, "Optical coupling of adjacent stripe-geometry junction lasers," Appl. Phys. Lett. **17**, 371–373 (1970).
6. E. M. Philipp-Rutz, "Spatially coherent radiation from an array of GaAs lasers," Appl. Phys. Lett. **26**, 475–477 (1975).
7. D. R. Scifres, R. D. Burnham, and W. Streifer, "Phase-locked semiconductor laser array," Appl. Phys. Lett. **33**, 1015–1017 (1978).
8. W. T. Tsang, R. A. Logan, and R. P. Salathe, "A densely packed monolithic linear array of GaAs-$Al_xGa_{1-x}As$ strip buried heterostructure laser," Appl. Phys. Lett. **34**, 162–165 (1979).
9. D. E. Ackley and R. W. H. Engelmann, "High-power leaky-mode multiple-stripe laser," Appl. Phys. Lett. **39**, 27–29 (1981).
10. J. Katz, E. Kapon, C. Lindsey, S. Margalit, U. Shreter, and A. Yariv, "Phase-locked semiconductor laser array with separate contacts," Appl. Phys. Lett. **43**, 521–523 (1983).
11. D. Botez and J. C. Connolly, "High-power phase-locked arrays of index-guided diode lasers," Appl. Phys. Lett. **43**, 1096–1098 (1983).
12. E. Kapon and J. Katz, "Supermode analysis of phase-locked arrays of semiconductor lasers," Opt. Lett. **10**, 125–127 (1984).
13. S. Wang, J. Z. Wilcox, M. Jansen, and J. J. Yang, "In-phase locking in diffraction-coupled phased-array diode lasers," Appl. Phys. Lett. **48**, 1770–1772 (1986).
14. Y. Huo and P. K. Cheo, "Analysis of transverse mode competition and selection in multicore fiber lasers," J. Opt. Soc. Am. B **22**, 2345–2349 (2005).
15. H. F. Talbot, "Facts relating to optical science No. IV," Philos. Mag. **9**, 401–407 (1836).
16. C. R. Fernández-Pousa, M. T. Flores-Arias, C. Bao, M. V. Pérez, and C. Gómez-Reino, "Talbot conditions, Talbot resonators, and first-order systems," J. Opt. Soc. Am. B **20**, 638–643 (2003).
17. J. R. Leger, M. L. Scott, and W. B. Veldkamp, "Coherent addition of AlGaAs lasers using microlenses and diffractive coupling," Appl. Phys. Lett. **52**, 1771–1773 (1988).
18. F. X. D'Amato, E. T. Siebert, and C. Roychoudhuri, "Coherent operation of an array of diode lasers using a spatial filter in a Talbot cavity," Appl. Phys. Lett. **55**, 816–818 (1989).
19. Y. Kono, M. Takeoka, K. Uto, A. Uchida, and F. Kannari, "A coherent all-solid-state laser array using the Talbot effect in a three-mirror cavity," IEEE J. Quantum Electron. **36**, 607–614 (2000).
20. A. M. Hornby, H. J. Baker, A. D. Colley, and D. R. Hall, "Phase locking of linear arrays of CO_2 waveguide lasers by the waveguide-confined Talbot effect," Appl. Phys. Lett. **63**, 2591–2593 (1993).
21. P. Glas, D. Fischer, M. Sandrock, M. Wrage, and T. Pertsch, "Bessel beam like emission characteristics of a neodymium-doped multicore fiber laser using a Talbot cavity," in *Conference on Lasers and Electro-Optics* (Optical Society of America, 2000), pp. 599–600.
22. M. Wrage, P. Glas, D. Fischer, M. Leitner, D. V. Vysotsky, and A. P. Napartovich, "Phase locking in a multicore fiber laser by means of a Talbot resonator," Opt. Lett. **25**, 1436–1438 (2000).
23. L. Michaille, C. R. Bennett, D. M. Taylor, T. J. Shepherd, J. Broeng, H. R. Simonsen, and A. Petersson, "Phase locking and supermode selection in multicore photonic crystal fiber lasers with a large doped area," Opt. Lett. **30**, 1668–1670 (2005).
24. P. K. Cheo, A. Liu, and G. G. King, "A high-brightness laser beam from a phase-locked multicore Yb-doped fiber laser array," IEEE Photon. Technol. Lett. **13**, 439–441 (2001).
25. M. Wrage, P. Glas, and M. Leitner, "Combined phase locking and beam shaping of a multicore fiber laser by structured mirrors," Opt. Lett. **26**, 980–982 (2001).
26. M. Wrage, P. Glas, D. Fischer, M. Leitner, N. N. Elkin, D. V. Vysotsky, A. P. Napartovich, and V. N. Troshchieva, "Phase-locking of a multicore fiber laser by wave propagation through an annular waveguide," Opt. Commun. **205**, 367–375 (2002).
27. T. Pertsch, P. Glas, M. Wrage, and F. Lederer, "An all-fiber phase locking setup for multicore fiber lasers," in *Conference on Lasers and Electro-Optics Europe* (IEEE, 2000), 314 pp.
28. P. Glas, D. Fischer, M. Leitner, T. Sandrock, M. Wrage, T. Pertsch, A. P. Napartovich, N. N. Elkin, A. G. Sukharev, V. N. Troshchieva, and D. V. Vysotsky, "Improvement of the emission characteristics of a multicore fiber laser using self

reproduction in a multimode interference device (MMI)," in *Conference on Lasers and Electro-Optics Europe* (IEEE, 2000), pp. 173.
29. Y. Huo, P. Cheo, and G. King, "Fundamental mode operation of a 19-core phase-locked Yb-doped fiber amplifier," Opt. Express **12**, 6230–6239 (2004).
30. L. Li, A. Schülzgen, S. Chen, V. L. Temyanko, J. V. Moloney, and N. Peyghambarian, "Phase locking and in-phase supermode selection in monolithic multicore fiber lasers," Opt. Lett. **31**, 2577–2579 (2006).
31. M. Wrage, P. Glas, M. Leitner, T. Sandrock, N. N. Elkin, A. P. Napartovich, and D. V. Vysotsky, "Reconstruction of field distributions of an active multicore fiber in multimode fibers," in *Laser Resonators III*, A. V. Kudryashov and A. H. Paxton, eds., Proc. SPIE **3930**, 212–221 (2000).
32. Fimmwave, Photon Design Inc., UK, http://www.photond.com/.
33. L. B. Soldano and E. C. M. Pennings, "Optical multi-mode interference devices based on self-imaging: principles and applications," J. Lightwave Technol. **13**, 615–627 (1995).
34. L. Li, A. Schülzgen, V. L. Temyanko, T. Qiu, M. M. Morrell, Q. Wang, A. Mafi, J. V. Moloney, and N. Peyghambarian, "Short-length microstructured phosphate glass fiber lasers with large mode areas," Opt. Lett. **30**, 1141–1143 (2005).
35. L. Li, A. Schülzgen, V. L. Temyanko, M. M. Morrell, S. Sabet, H. Li, J. V. Moloney, and N. Peyghambarian, "Ultracompact cladding-pumped 35-mm-short fiber laser with 4.7-W single-mode output power," Appl. Phys. Lett. **88**, 161106 (2006).
36. G. G. King and P. K. Cheo, "M^2 measurements of multicore fiber laser array," in *Technical Digest of the 16th Solid State & Diode Laser Technology Review* (Directed Energy Professional Society, 2003), paper P-12.